Synthesis, Characterization, Biological and Docking Simulations of 4-(Benzylideneamino) Benzoic Acids①

HAMID Aziz[a] AAMER Saeed[a②] FARUKH Jabeen[b, c] ABDUL Basit[d] IRFAN Zia Qureshi[d]
ABDUL Aziz[d] ATIF Haroon[e] ASHFAQ Ur Rehman[f, g]

[a] (*Department of Chemistry Quaid-I-Azam University Islamabad* 45320, *Pakistan*)

[b] (*Computation, Science, Research and Development Organization,* 1401, 2485 *Hurontraio Street, Mississauga, ON, Ca, L5A2G6*)

[c] (*Department of Biology, Laurentian University,* 935 *Ramsey Lake Road, Sudbury, ON, Canada P3E2C6*)

[d] (*Department of Animal Sciences Quaid-I-Azam University Islamabad* 45320, *Pakistan*)

[e] (*Department of Microbiology Quaid-I-Azam University Islamabad* 45320, *Pakistan*)

[f] (*Department of Biochemistry, Shankar Campus, Abdul Wali Khan University, Mardan* 23200, *Khyber Pukhtoonkhwa, Pakistan*)

[g] (*Department of Bioinformatics and Biostatistics, Shanghai Jiaotong University, Shanghai* 200240, *China*)

ABSTRACT The present research paper presents the synthesis, characterization, biological and computational studies of 4-(benzylideneamino) benzoic acid derivatives (**3a**～**3g**). Derivatives **3a**～**3c** displayed best antidiabetic potential with a glucose-lowering effect compared to the reference drug Glibenclamide. Biochemical parameters including plasma glucose, serum triglycerides, cholesterol, alanine amino transferase and aspartate amino transferase levels showed significant alterations in concentrations relative to the control. Similarly, the derivatives **3a**, **3d** and **3e** displayed potent *in vitro* antibacterial potential. Molecular docking simulations delineated that the ligands and complexes were stabilized at the active site by electrostatic and hydrophobic forces, consistent with the corresponding experimental results. *In silico* study of the binding pattern predicted that the synthesized ligands, **3d** and **3a** could serve as a potential surrogate for hit-to-lead generation and the design of novel antibacterial drugs.

Keywords: antidiabetic, biochemical, cholesterol, glibenclamide, simulations;
DOI: 10.14102/j.cnki.0254–5861.2011–2871

1 INTRODUCTION

Diabetes mellitus (DM) is a group of life style-related, non-communicable, endocrinological and metabolic disorder with diverse etiologies[1]. DM is characterized by hyperglycemia resulting from defects in insulin secretion leading to incomplete metabolism of carbohydrates, lipids and proteins[2]. The prevalent type-II diabetes is a metabolic syndrome characterized by high blood glucose level because of hectic lifestyle. Type-I diabetes is resulted because of no insulin production and causes frequent urination, increased thirst and hunger[3]. Recent research suggests the loss of functional β-cell mass through apoptosis and advanced glycation end products as the leading cause of developing DM[4]. In this regard, nitrogen containing heterocycles particularly Schiff bases (SB) are revealed as potent antidiabetic agents[5-7].

SB serves as a promising source for the rational design of biologically relevant heterocycles including thiazolidinone[8], azetidone[9], oxadiazole, benzoxazoles[10], and quinolone[11]. SB contain azomethine linkages and display potent biological profile like anticancer[12], antituberculosis[13], antimicrobial[14], antipyretics[15], antiproliferative[16], and antidiabetic[17]. They serves as excellent chelating agents[10, 18]. The electrophilic carbon and nucleophilic nitrogen atoms interact with nucleophiles and electrophiles that lead to enzyme inhibition. Similarly, tumor cells selectively hydrolyze SB to serve as alkylating agents while the free amines simultaneously act as antimetabolites[10]. Rhodopsin is an azomethine pigment

Received 9 May 2020; accepted 2 December 2020

① Financial support of the Higher Education Commission (HEC) Pakistan, by awarding indigenous fellowship batch-1 phase-II for M.Phil leading to Ph.D

② Corresponding author. E-mail: aamersaeed@yahoo.com

formed biochemically by the reaction of formyl group of *cis*-retinal with an amine group of an Apo protein opsin. The azomethine linkages of pyridoxal phosphate coenzyme play a pivotal role in the metabolic pathways of biologically essential amino acids[16, 19, 20]. Azomethine linkages serve as useful substrates to produce conducting materials as well as polymers[21, 22]. Reactive oxygen and nitrogen species cause oxidative stresses and damage cellular structures. Azomethine linkages provide protection against oxidative damage and consequently help to prevent DM[23, 24]. In this regard, azomethine linkages of isatin derivatives are reported as potent *in vitro* antiglycation agents[25]. Similarly, Vanco et al. reports the *in vivo* antidiabetic potential of *N*-salicylidene-*β*-alanine azomethine linkages[26].

Thus keeping in view the harmful effects of DM and the potent antidiabetic potential of amino-based heterocycles, there is an utmost need for the design and synthesis of SB. In this regard, the present paper reports the facile synthesis, spectroscopic characterization, biological and computational evaluation of 4-(benzylideneamino) benzoic acid derivatives (**3a**～**3g**).

2 EXPERIMENTAL

2. 1 Materials and method

All the chemicals used were obtained from commercial suppliers. NMR spectra were recorded using Bruker NMR spectrometer at 300 MHz (^{1}H) as well as 75 MHz (^{13}C). NMR chemical shifts are expressed in ppm scale (δ) relative to the reference standard TMS and DMSO-d_6 as a solvent. The coupling constants *J* were measured in Hertz. Multiplicities in ^{1}H NMR are reported as broad (b), singlet (s), doublet (d), triplet (t) and multiplet (m). FT-IR spectra were recorded on the Vertex 70 Bruker apparatus. Elemental analysis (CHNS) was performed to determine the percentage of each element. The reaction was monitored by TLC on 2.0cm × 5.0cm aluminium sheets (silica gel, 60F254 Merck).

2. 2 Synthesis of 4-(benzylideneamino) benzoic acid derivatives (3a～3g)

The syntheses of 4-(benzylideneamino) benzoic acid derivatives (**3a**～**3g**) were performed as reported elsewhere[27]. Briefly, substituted aldehyde (0.1 mol) was completely dissolved in dry distilled ethanol (5.0 mL) at reflux in a 250 mL round bottom flask containing a drop of concentrated sulphuric acid. A solution of 4-aminobenzoic acid (0.1 mol) prepared in dry distilled ethanol (5.0 mL) was added to the reaction mixture and the reaction was refluxed for next 5 hours (hrs). During the reaction, TLC was constantly used to monitor the progress of the reaction. The reaction mixture was cooled to room temperature, which resulted in the formation of solid precipitates of the target products.

2. 2. 1 4-(3-Methoxy, 4-hydroxybenzylideneamino)benzoic acid (3a)

Yield: 75%; m.p: 248 ℃; color: white; FT-IR (ATR, cm^{-1}): 3000, 2913(sp^2 C–H stretch), 2954, 2855 (sp^3 C–H stretch), 1678(COO$^-$, asymmetric), 1673, 1567, 1420(C=C, aromatic), 1593(HC=N), 1420 (COO$^-$ symmetric), 1284(C–N); ^{1}H NMR (DMSO-d_6), 11.08 (b, s, 1H, COOH), 8.50 (d, 2H, *J* = 8.20 Hz, Ar), 8.48 (s, 1H, HC=N), 7.76 (d, 2H, *J* = 8.20 Hz, Ar), 7.63 (d, 1H, *J* = 7.92 Hz, Ar), 7.01 (d, 1H, *J* = 7.92 Hz, Ar); 6.94 (s, 1H, Ar), 3.72 (s, 3H, OCH_3); ^{13}C NMR (DMSO-d_6), 169.84 (C=O), 160.22 (HC=N), 158.50 (Ar), 152.10 (Ar), 148.20 (Ar), 132.56 (Ar), 130.70 (Ar), 129.80 (Ar), 129.10 (Ar), 128.60 (Ar), 124.20 (Ar), 122.84 (Ar), 52.78 (O–C). Anal. Calcd. (%) for $C_{15}H_{13}NO_4$: C, 66.41; H, 4.83; N, 5.16. Found (%): C, 66.35; H, 4.88; N, 5.21.

2. 2. 2 4-(2-Hydroxybenzylideneamino)benzoic acid (3b)

Yield: 70%; m.p: 269 ℃; color: yellow; FT-IR (ATR, cm^{-1}): 2970(sp^2 C–H stretch), 1679(COO$^-$, asymmetric), 1620, 1568, 1496(C=C, aromatic), 1597(HC=N), 1428 (COO$^-$ symmetric), 1285(C–N); ^{1}H NMR (DMSO-d_6), 11.13 (b, s, 1H, COOH), 8.25 (d, 2H, *J* = 8.22 Hz, Ar), 8.20 (d, 2H, *J* = 8.22 Hz, Ar), 8.16 (s, 1H, HC=N), 7.69 (d, 2H, *J* = 8.10 Hz, Ar), 7.12 (t, 1H, *J* = 8.0 Hz, Ar), 6.83 (t, 1H, *J* = 8.0 Hz, Ar); ^{13}C NMR (DMSO-d_6), 170.20 (C=O), 158.46 (HC=N), 158.43 (Ar), 150.10 (Ar), 141.45 (Ar), 139.87 (Ar), 128.56 (Ar), 127.34 (Ar), 125.63 (Ar), 122.10 (Ar), 121.30 (Ar). Anal. Calcd. (%) for $C_{14}H_{11}NO_3$: C, 69.70; H, 4.60; N, 5.81. Found (%): C, 69.79; H, 4.51; N, 5.80.

2. 2. 3 4-(4-Methylbenzylideneamino)benzoic acid (3c)

Yield: 75%; m.p: 235 ℃; color: white; FT-IR (ATR cm^{-1}): 3033, 2981 (sp^2 C–H stretch), 2943, 2876 (sp^3 C–H stretch), 1681(COO$^-$, asymmetric), 1660, 1560, 1440 (C=C, aromatic), 1593(HC=N), 1422(COO$^-$ symmetric), 1284(C–N); ^{1}H NMR (DMSO-d_6), 11.28 (b, s, 1H, COOH), 8.58 (d, 2H, *J* = 8.21 Hz, Ar), 8.38 (s, 1H, HC=N), 7.69 (d, 2H, *J* = 8.21 Hz, Ar), 7.68 (d, 2H, *J* = 8.15 Hz, Ar), 7.01 (d, 2H, *J* = 8.15 Hz, Ar); 2.29 (s, 3H, CH_3); ^{13}C NMR (DMSO-d_6), 168.40 (C=O), 159.21 (HC=N), 157.50 (Ar), 142.20 (Ar), 132.10 (Ar), 130.40 (Ar), 129.20 (Ar), 128.50 (Ar), 128.10 (Ar), 122.40 (Ar), 25.50 (C–H). Anal. Calcd. (%) for $C_{15}H_{13}NO_2$: C, 75.30; H, 5.48; N, 5.85. Found (%): C, 75.35; H, 5.43; N, 5.80.

2. 2. 4 4-(4-Nitrobenzylideneamino)benzoic acid (3d)

Yield: 85%; m.p: 290 ℃; color: red; FT-IR (ATR, cm^{-1}): 2970(sp^2 C–H stretch), 1670(COO^-, asymmetric), 1632, 1599, 1514(C=C, aromatic), 1589(HC=N), 1426(COO^- symmetric), 1285(C–N); ^{1}H NMR (DMSO-d_6), 11.13 (b, s, 1H, COOH), 8.63 (s, 1H, HC=N), 8.22 (d, 2H, *J* = 8.31 Hz, Ar), 7.55 (d, 2H, *J* = 8.25 Hz, Ar), 8.35 (d, 2H, *J* = 8.31 Hz, Ar), 7.15 (d, 2H, *J* = 8.25 Hz, Ar); ^{13}C NMR (DMSO-d_6), 170.20 (C=O), 158.46 (HC=N), 158.43 (Ar), 150.10 (Ar), 141.45 (Ar), 139.87 (Ar), 128.56 (Ar), 127.34 (Ar), 125.63 (Ar), 121.30 (Ar). Anal. Calcd. (%) for $C_{14}H_{10}N_2O_4$: C, 62.22; H, 3.73; N, 10.37. Found (%): C, 62.17; H, 3.75; N, 10.40.

2. 2. 5 4-(4-Chlorobenzylideneamino) benzoic acid (3e)

Yield: 80%; m.p: 176 ℃; color: yellow; FT-IR (ATR, cm^{-1}): 3013, 2980(sp^2 C–H stretch), 1678(COO^-, asymmetric), 1625, 1588, 1489(C=C, aromatic), 1425(COO^- symmetric), 1588 (HC=N), 1300 (C–N); ^{1}H NMR (DMSO-d_6), 11.10 (b, s, 1H, COOH), 8.56 (s, 1H, HC=N), 8.20 (d, 2H, *J* = 8.23 Hz, Ar), 7.80 (d, 2H, *J* = 8.13 Hz, Ar), 7.50 (d, 2H, *J* = 8.23 Hz, Ar), 7.15 (d, 2H, *J* = 8.13Hz, Ar); ^{13}C NMR (DMSO-d_6), 170.23 (C=O), 158.43 (HC=N), 158.31 (Ar), 140.16 (Ar), 131.45 (Ar), 129.67 (Ar), 128.60 (Ar), 127.20 (Ar), 126.30 (Ar), 125.12 (Ar). Anal. Calcd. (%) for $C_{14}H_{10}ClNO_2$: C, 64.75; H, 3.88; N, 5.39. Found (%): C, 64.68; H, 3.93; N, 5.56.

2. 2. 6 4-(3-Hydroxy, 4-methoxyylbenzyli-deneamino)benzoic acid (3f)

Yield: 75%; m.p: 180 ℃; color: white; FT-IR (ATR cm^{-1}): 3089, 2954(sp^2 C–H stretch), 2950, 2860(sp^3 C–H stretch), 1677(COO^-, asymmetric), 1670, 1565, 1425(C=C, aromatic), 1589(HC=N), 1429 (COO^- symmetric), 1284(C–N); ^{1}H NMR (DMSO-d_6), 11.08 (b, s, 1H, COOH), 8.50 (d, 2H, *J* = 8.30 Hz, Ar), 8.48 (s, 1H, HC=N), 7.76 (d, 2H, *J* = 8.30 Hz, Ar), 7.63 (d, 2H, *J* = 8.20 Hz, Ar), 7.01 (t, 1H, *J* = 8.25 Hz, Ar), 3.72 (s, 3H, OCH_3); ^{13}C NMR (DMSO-d_6), 169.84 (C=O), 160.22 (HC=N), 158.50 (Ar), 152.10 (Ar), 148.20 (Ar), 132.56 (Ar), 130.70 (Ar), 129.80 (Ar), 129.10 (Ar), 128.60 (Ar), 124.20 (Ar), 122.84 (Ar), 52.78 (O–C). Anal. Calcd. (%) for $C_{15}H_{13}NO_4$: C, 66.41; H, 4.83; N, 5.16; Found: C, 66.35; H, 4.87; N, 5.22.

2. 2. 7 4-(4-Florobenzylideneamino)benzoic acid (3g)

Yield: 70%; m.p: 204 ℃; color: yellow; FT-IR (ATR, cm^{-1}): 3000(sp^2 C–H stretch), 1678(COO^-, asymmetric), 1625, 1588, 1489(C=C, aromatic), 1581 (HC=N), 1428(COO^- symmetric), 1293(C–N); ^{1}H NMR (DMSO-d_6), 11.10 (b, s, 1H, COOH), 8.52 (d, 2H, *J* = 8.21 Hz, Ar), 8.40 (s, 1H, HC=N), 7.74 (d, 2H, *J* = 8.21 Hz, Ar), 7.58 (d, 2H, *J* = 7.90 Hz, Ar), 7.08 (d, 2H, *J* = 7.90 Hz, Ar); ^{13}C NMR (DMSO-d_6), 170.20 (C=O), 158.35 (HC=N), 158.50 (Ar), 140.16 (Ar), 131.43 (Ar), 129.76 (Ar), 128.65 (Ar), 126.31 (Ar), 125.20 (Ar), 123.12 (Ar). Anal. Calcd. (%) for $C_{14}H_{10}FNO_2$: C, 69.13; H, 4.14; N, 5.76. Found: C, 69.10; H, 4.18; N, 5.49.

2. 3 *In vivo* antidiabetic assay

For this purpose, thirty-six BALB/c healthy adult male mice (average weight = 33.8±0.8 gm) were procured from the National Institute of Health Islamabad. Four animals were housed per cage and had free access to standard diet of rodents and drinking water. Standard temperature of 28 ℃ and 12 hL:12 hD photoperiod were maintained throughout. Diabetic models were made through single intraperitoneal injection (*i.p.*) dose (150 mg/kg b.w) of Alloxan mono-hydrate[17, 28]. The animals were checked for diabetes after 24 hrs of Alloxan monohydrate administered to 12 hrs fasted mice. Diabetic level was achieved at fasting plasma glucose concentration > 200 mg/dL. For antidiabetic screening, a total of nine experimental groups were constituted. Seven groups were treated with seven different derivatives at the dose of 5 mg/kg b.w dissolved in DMSO. The remaining two groups, positive and negative control groups, were treated with Glibenclamide (10 mg/kg b.w in DMSO) and DMSO, respectively. The screening derivatives were intraperitoneally administered through a single injection on day 2. Blood was obtained from caudal vein at nine different times; −1 hrs (pre-alloxan), 0 hrs (postalloxan) and 1～7 hrs after treatment with doses. Plasma glucose level was determined with dextrostix strips using glucometer. Serum triglycerides, cholesterol, alanine amino transferase (ALT) and aspartate amino transferase (AST) levels were estimated through commercially available kits using the standard calorimetry procedure[29].

2. 4 Antibacterial assay

Antibacterial assay of the derivatives (**3a** ～ **3g**) was determined by agar disc diffusion method[30]. Briefly, two gram-positive (*Staphylococcus aureus* and *Streptococcus pneumoniae*) and three gram-negative (*Escherichia coli*, *Enterobacter aerogenes* and *Klebsiella pneumoniae*) were cultured in a nutrient broth for 24 hrs at 37 ℃. The cultured strains were used as inoculums (1%) and were added to the nutrient agar medium at 45 ℃, poured into sterile Petri plates and allowed to solidify. 5 mL of the derivative (200 mg/mL, final concentration) was poured on sterile filter paper discs (4 mm) and placed on nutrient ager plates, respectively. Amikacin and DMSO were used as positive and negative

controls, respectively. The assay was performed in triplicate and the plates were incubated at 37 ℃ for 24～48 hrs. The antibacterial potential was determined by measuring the diameter of zones of inhibition (ZOI, mm) using Vernier caliper.

2. 5 Computational studies

2. 5. 1 Methodology

Molecular operating environment (MOE)[31] was used for MD studies against antibacterial target E. coli 16S-rRNA A-site. First, 3*D* structures were generated using the builder tool executed in MOE package. Next, the derivatives were protonated and energy-minimized using the default parameters of MOE (gradient: 0.05, force field: MMFF94X). 3*D* structure of the target protein was retrieved from protein databank (PDB code 1j7t). The water molecules were removed and 3*D* protonation was carried out. Afterwards, the protein was energy-minimized using the MOE package. For docking studies, default parameters of the MOE package *i.e.*, placement: triangle matcher, rescoring 1: London dG, refinement: forcefield, and rescoring 2: GBVI/WSA were used. For each ligand, ten conformations could be fashioned and the top-ranked conformations based on docking score were selected for additional analysis.

2. 5. 2 All-atom MD simulations

For MD simulations, all-atom simulations and reasonable analysis procedures were conducted in by AMBER18 software package. The LEaP module was used to add hydrogen atoms to both crystallographic structures. Counter-ions (Na^+ and Cl^-) were added to maintain the system neutrality. All systems were solvated in a truncated octahedral box of TIP3P water model with 10 Å buffer. Particle Mesh Ewald (PME) method was used to treat long-range electrostatic interactions, and ff12SB force field was used for all simulations. All the bonds involving hydrogen atoms were constrained with SHAKE algorithm. PMEMD of CUDA version was used to accelerate all the MD simulations. Steepest descent method was used to minimize the solvated systems for 20000-step, then 400 ps heating, and 200 ps equilibration in the NVT ensemble. The default parameters of the Langevin thermostat method were used for the heating and equilibration runs with a time step of 2 fs, and for the production runs under NPT ensemble at 298 K with a time step of 2 fs in Berendsen's thermostat and barostat.

2. 6 Statistical analysis

One-way analysis of variance (ANOVA) was used for data analysis using Sigma Plot (Version 12.0), Post hoc Tukey-Kramer test, where the test for normality failed ANOVA on ranks test was applied. Statistically significant difference was considered where $p < 0.05$. Data are presented as line or bar graphs Graph-Pad Prism (Version 5.0).

3 RESULTS AND DISCUSSION

3. 1 Chemistry

The 4-(benzylideneamino) benzoic acid derivatives (**3a**～**3g**) were synthesized by dissolving substituted benzaldehydes in dry distilled ethanol containing a drop of concentrated sulphuric acid at reflux. After an hr, ethanolic solution of 4-aminobenzoc acid was added and the reaction mixture was again refluxed for another 5 hrs (scheme 1). The reaction progress was monitored by TLC in a (chloroform:methanol, 7:3) solvent system. After 5 hrs, the reaction was stopped and cooled to room temperature, resulting in the formation of solid precipitates which were filtered and recrystallized from a mixture of ethanol and DCM at room temperature[27].

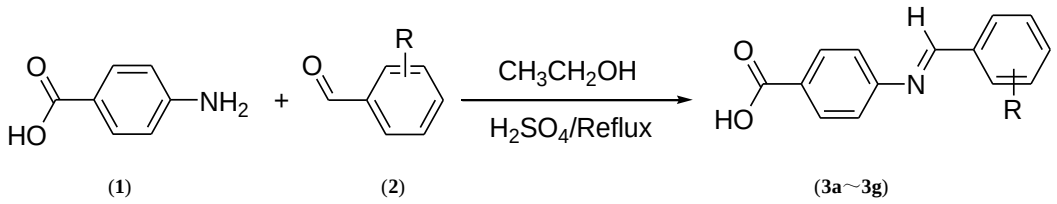

(**1**) (**2**) (**3a**～**3g**)

Scheme 1. Synthetic scheme and structures of the synthesized 4-(benzylideneamino) benzoic acid derivatives (3a～3g)

Table 1. Structures of the Synthesized 4-(Benzylideneamino) Benzoic Acid Derivatives (3a～3g)

S. No.	Compound	R	S. No.	Compound	R
1	**3a**	3-OCH_3, 4-OH	5	**3e**	4-Cl
2	**3b**	2-OH	6	**3f**	3-OH, 4-OCH_3,
3	**3c**	4-CH_3	7	**3g**	F
4	**3d**	4-NO_2	…	**…**	**…**

3. 2 Spectroscopic studies

Structure assignments of the synthesized 4-(benzylidene-amino) benzoic acid derivatives (**3a**～**3g**) were based on their spectroscopic data (FT-IR, ^{1}H NMR, ^{13}C NMR) and elemental analysis (CHNS). The derivatives (**3a**～**3g**) gave satisfactory C, H, N and S analyses data highly aligned with their structural formulae. FT-IR spectra of the derivatives (**3a**～**3g**) display absorption peaks in the range of 2900～3100 cm^{-1} being assigned to the sp^2 hybridized CH stretch. The COOH group protons appear in the ^{1}H NMR spectra as broader signals in the range of 11.0～11.28 ppm. FT-IR spectra of the derivatives (**3a**～**3g**) display peaks in the range of 1581～1597cm^{-1} for the subsequent azomethine linkages (HC=N) which are evident as sharp singlets at 8.16～8.63 and 158.31 ～ 160.22 ppm in their ^{1}H and ^{13}C NMR spectra[28].

3. 3 *In vivo antidiabetic* assay

When mice were treated with the derivatives (**3a**～**3g**), the concentration of glucose was altered noticeably ($F = 43.986$, $P < 0.001$). **3a**, **3b** and **3c** considerably ($P < 0.001$, Fig. 1a～1c) while **3d** and **3f** slightly but significantly decreased the glucose concentrations compared to the negative control ($P < 0.05$). In contrast, **3f** and **3g** did not show any significance effect on the glucose level ($P > 0.05$), (Fig. 1d).

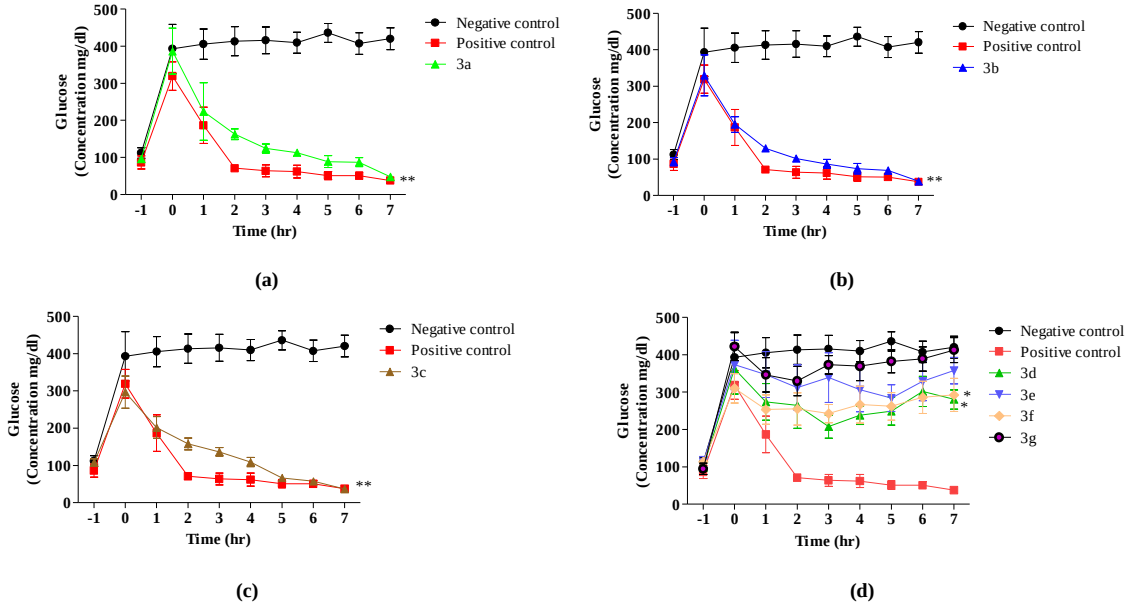

Fig. 1. Glucose concentration of mice altered significantly when treated with (3a～3g).
Data are presented as mean ± SE, $^*P < 0.05$; $^{**}P < 0.001$

3. 4 Biochemical parameters

Significant alteration was found in total cholesterol after treatment of mice ($F = 53.973$, $P < 0.001$). **3c**, **3d** and **3e** substantially decreased the cholesterol level by comparison with both positive and negative controls ($P < 0.001$ and $P > 0.05$). In contrast, **3b** and **3f** caused an increase as compared to both the controls ($P < 0.001$ and $P < 0.05$), whereas **3a** and **3g** increased the cholesterol level compared to positive control and decreased versus negative control ($P < 0.001$ and $P < 0.05$) (Figs. 2a and 2b). Serum triglyceride level also revealed significant alterations ($F = 916.414$, $P < 0.001$). The serum triglyceride level of mice decreased with **3a** and **3b** while increased with **3c**～**3g** ($P < 0.001$ and $P < 0.05$) (Figs. 2a and 2b).

The ALT and AST levels of blood serum were also affected ($F = 43.894$, $P < 0.001$); i.e. their levels rose with **3a**～**3e** and **3f** ($P < 0.001$ and $P < 0.05$) while **3g** had no effect ($P > 0.05$, Figs. 3a and 3b).

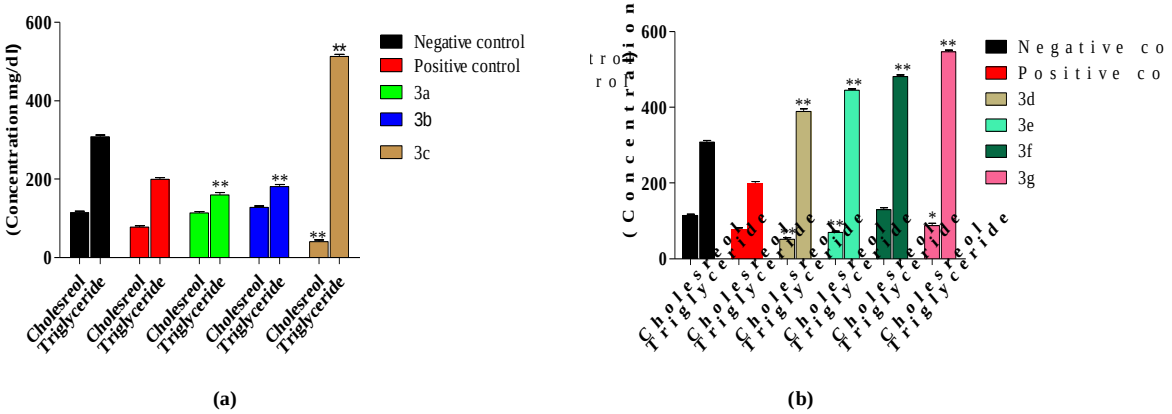

(a) **(b)**

Fig. 2. Cholesterol and triglyceride levels of mice altered significantly when administered with (3a～3g). Data are presented as mean ± SE, $^{*}P < 0.05$ and $^{**}P < 0.001$

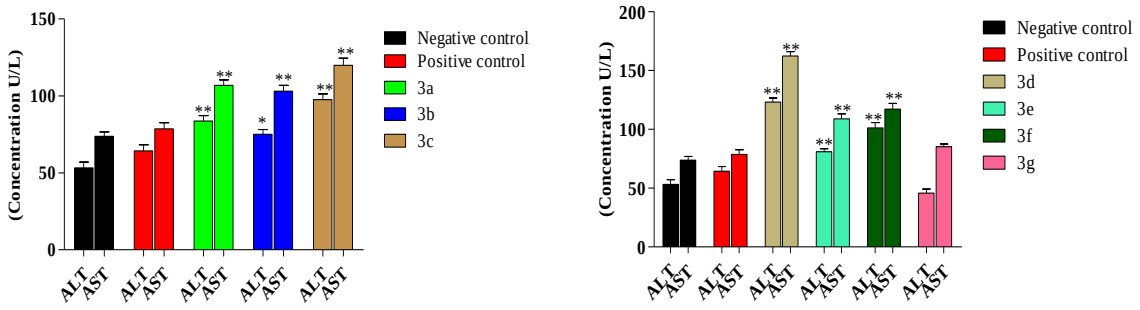

(a) **(b)**

Fig. 3. Concentration of ALT and AST of mice showed significant alteration after treatment with (3a～3g). Data are presented as mean ± SE, $^{*}P < 0.05$ and $^{**}P < 0.001$

To conclude, the derivatives (**3a**～**3d, 3f**) showed glucose lowering effect compared to the reference drug Glibanclamide and the remaining derivatives **3e** and **3g** were found to be lacking antihyperglycemic activity. Likewise, the biochemical parameters showed significant alterations upon treatments. **3a**, **3c**, **3e** and **3g** showed high level of anticholesterol potency, while only **3a** and **3b** caused a decrease in the triglycerides level. **3c**～**3g** increased the triglycerides level. The results obtained are consistent with the literature, indicating the metabolic alterations of mice when the derivatives were administered[17, 28, 29]. Except **3g**, all the derivatives increased the ALT and AST levels. These results obtained show similarity with a diphenyl diselenide, diphenyl ditelluride and Ebselen caused potential renal and hepatic toxicity in rats and mice as reported elsewhere[29]. Thus, based on the results obtained, it can be concluded that the derivatives (**3a** ～ **3g**) are also hepatotoxic when administered to mice at the dose of 5 mg/kg.

3. 5 Antibacterial activity

Antibacterial potential of the derivatives (**3a**～**3g**) was determined from agar disc diffusion method. The derivatives (**3a**～**3g**) were employed in different zones and the results in terms of their ZOI were determined (Table 2). The derivative **3a** showed higher antibacterial potential against all the screened strains. The antibacterial potential was found to be higher than the positive control Amikacin against the *Enterobacter aerogenes*. The derivative **3d** showed moderate potential against all the bacterial strains. Similarly, the derivative **3e** showed good antibacterial activity against all the screened strains except *Streptococcus pneumoniae*, where no activity was observed. Unlike **3e**, **3b** showed antibacterial activity only against *Staphylococcus aureus* and *Enterobacter aerogenes*. The remaining derivatives were found to be less potent against the screened bacterial strains[30].

Table 2. Antibacterial Assay Results of the Screened 4-(Benzylideneamino) Benzoic Acid Derivatives (3a～3g)

S. No.	Compound	Zone of inhibition (mm) at 200 (mg/mL)				
		E. coli	*K. pneumoniae*	*S. aureus*	*S. pneumoniae*	*E. aerogenes*
1	Amikacin	19	19	30	20	22
2	DMSO	0	0	0	0	0
3	**3a**	17	16	14	12	24
4	**3b**	0	0	9	0	16
5	**3c**	7	0	0	0	0
6	**3d**	14	12	16	15	18
7	**3e**	13	10	7	0	9
8	**3f**	9	0	0	10	9
9	**3g**	0	0	9	0	0

3. 6 Molecular docking

Binding modes of the derivatives (**3a** ～ **3g**) against antibacterial target were evaluated from *in silico* analysis. Crystal structure solved by Eric Westhof group[32] at 2.5 Å resolution (PDB code 1j7t) which includes the antibiotic docked into the eubacterial ribosomal decoding A site was chosen for antibacterial assay. MD results revealed the most potent derivatives (**3a**, **3d**) possess the best activity against the target enzymes both *in silico* and experimentally. In case of (**3a**, **3d**), the crystal structure revealed each RNA, and the fragment contains two A sites inserted between Watson-Crick pairs. **3a** and **3d** interact in an enlarged deep groove created by two bulging and one unpaired adenines (Fig. 4a) and adopted favorable interactions. The receptor-ligand interaction (RLI) profile for **3d** revealed a typical interaction (A17) with target and some other, *i.e.*, G15 and A16, respectively (Fig. 4c). **3a** adopted total three interactions: π-stacking with the 1,6-dihydropyrimidine ring of G15, with the (O) of OP3 of A17 and with the NH_2 of A29 (Fig. 4b). The high potency of **3a** over others might be due to the new methoxide group with OH over benzene compared with **3d**, which only has the 1-nitrobenzene group. Even though in both cases, the substituted group belongs to deactivating category, it withdraws the electron from benzene ring and further triggers the partial positive charge at benzene ring, and this effect further enhances the potency of other atoms to adopt interactions with other residues to gain stability and enhance the activity at a different level. These results delineate that the molecules possessing double deactivating group at benzene ring have the tendency to trigger the partial positive charge over benzene ring, thus further activating other atoms to adopt favorable interactions with crucial residues and subsequently enhancing the corresponding activity.

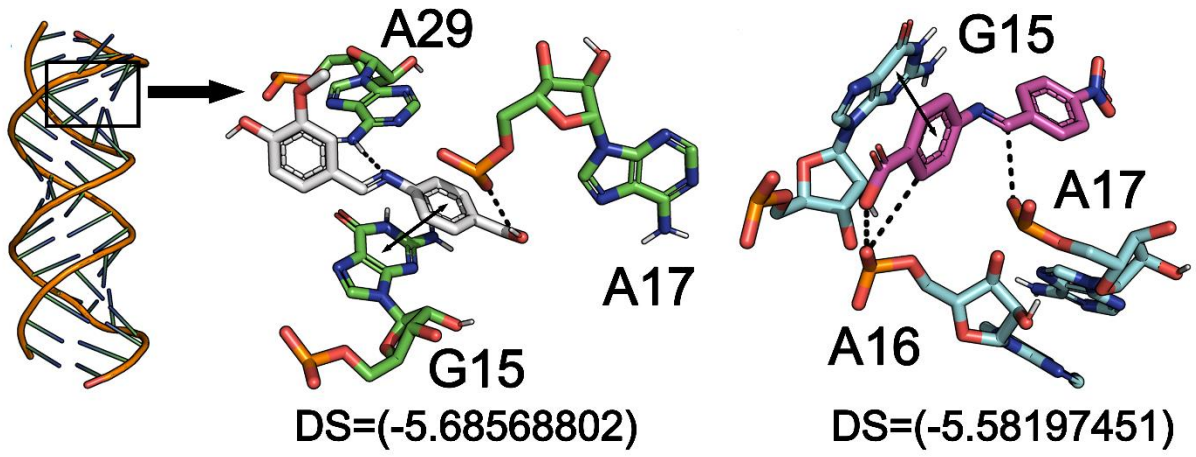

(a) **(b)** **(c)**

Fig. 4. RLI profile for the potent derivatives (3a, 3d) against antibacterial targets. (a) Surface representation of antibacterial target (PDB ID 1j7t). Binding mode of the high potent molecule (b) for 3a and (c) for 3d

3. 7 All-atom molecular dynamics simulation

To further validate the results of docking, MD simulation was performed[33, 34]. A total of 20ns simulations were performed in order to categorize the internal motion and interaction of the derivatives (**3a**, **3d**). The root-mean-square-deviation (RMS*d*) was calculated to validate the stability of the simulations, which was a key parameter for evaluating the equilibrium of MD trajectories for the primary chain atoms of the protein system along the MD simulations. The amplitude of the RMS*d* curve fluctuation is negatively correlated with the protein's stability: the lower the fluctuation, the more stable the protein structure. The RMS*d* value of the backbone atoms for both derivatives was calculated and their results are shown (Fig. 5). The results indicate the RMS*d* value of **3a** as compared to **3d** for antibacterial assay as shown in Fig. 5a. Initially, the curve gradually increases (15 ns) and is highly fluctuated but becomes stable after 20 ns. The results show less fluctuation, which indicate that the trajectories generated during 20 ns are stable. Therefore, the following analysis was obtained from the 20ns trajectories, which shows that **3a** strongly inhibited the target (antibacterial) and bonded explicitly to the binding site. The derivative **3d** is loosely bound and inhibits the activity and hence is considered as a second inhibitor.

To determine how the derivatives (**3a, 3d**) influence the dynamics of the side chain of the target protein residues, the residues fluctuation in terms of root-mean-square-fluctuation (RMS*f*) was analyzed. The results of RMS*f* were like the RMS*d* value. **3a** shows strong binding with the active site residues (G15, A17, and A29), so the fluctuation is higher in the binding site and hence shows the best activity against antibacterial target (Fig. 5b), while in comparison to the residue's fluctuation with **3d**, fewer residues fluctuation was observed, which might indicate the lesser activity and interaction within the active pocket (Fig. 5b).

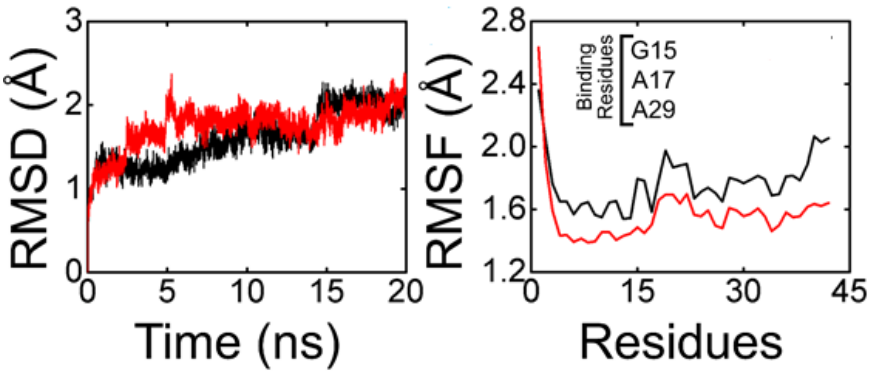

(a) **(b)**

Fig. 5. (a) Superposed RMSd graphs for 3a (black) and 3d (red) against the anti-bacterial target. The superposed RMSf graphs (b) for 3a (black) and 3d (red) against antibacterial target

4 CONCLUSION

The current research paper presents the successful synthesis, characterization, biological and computational analysis of 4-(benzylideneamino) benzoic acid derivatives (**3a**～**3g**). The derivatives (**3a**～**3c**) possess strong *in vivo* antidiabetic activity and may be processed as potent antidiabetic candidate while the remaining derivatives (**3d**～**3g**) lack antidiabetic response. The derivatives (**3a**～**3g**) were found to be hepatotoxic at the present dose level and cause metabolic abnormality. Further detailed studies, therefore, are required to check the efficacy and safety of the derivatives (**3a**～**3g**) at different dose levels. They have minimum side effects, and will be less toxic and can be processed as alternative drug candidates for diabetes other than the currently available drugs. MD simulations of the derivatives (**3a**～**3g**) against RNA provided further insight into the mode of action, mechanism of the inhibition and inhibitory potential of the drug-like molecules. Derivatives **3d** and **3a** exhibited better inhibitory potential against both the targets. These ligands stabilize themselves inside the active site through tremendous electrostatic and hydrophobic interactions. MD simulations further ascertained the interaction of these molecules with both the targets.

REFERENCES

(1) Upadhyay, R. K. Anti-arthritic potential of plant natural products; its use in joint pain medications and anti-inflammatory drug formulations. *Int. J. Green Pharm.* **2016**, 10, S120−S130.

(2) Puranik, N. V.; Puntambekar, H. M.; Srivastava, P. Antidiabetic potential and enzyme kinetics of benzothiazole derivatives and their non-bonded interactions with α-glucosidase and α-amylase. *Med. Chem. Res.* **2016**, 25, 805−816.

(3) Gin, H.; Rigalleau, V. Post-prandial hyperglycemia. Post-prandial hyperglycemia and diabetes. *Diabetes. Metab.* **2000**, 26, 265−272.

(4) American Diabetes Association. Diagnosis and classification of diabetes mellitus. *Diabetes Care* **2014**, S81−90.

(5) Schiff, H. The syntheses and characterization of Schiff base. *Ann. Chem. Suppl* 3 **1864**, 343−349.

(6) da Silva, C. M.; da Silva, D. L.; Modolo, L. V.; Alves, R. B.; de Resende, M. A.; Martins, C. V.; de Fátima, Â. Schiff bases: a short review of their antimicrobial activities. *J. Adv. Res.* **2011**, 2, 1−8.

(7) Chakraborti, A. K.; Bhagat, S.; Rudrawar, S. Magnesium perchlorate as an efficient catalyst for the synthesis of imines and phenylhydrazones. *Tetrahedron Lett.* **2004**, 45, 7641−7644.

(8) Küçükgüzel, G.; Kocatepe, A.; De Clercq, E.; Şahin, F.; Güllüce, M. Synthesis and biological activity of 4-thiazolidinones, thiosemicarbazides derived from diflunisal hydrazide. *Eur. J. Med.* **2006**, 41, 353−359.

(9) Kalsi, R.; Shrimali, M.; Bhalla, T. N.; Barthwal, J. P. Synthesis and anti-inflammatory activity of indolyl azetidinones. *Indian J. Pharm. Sci.* **1990**, 52, 129−134.

(10) Hameed, A.; al-Rashida, M.; Uroos, M.; Abid, A. S.; Khan, K. M. Schiff bases in medicinal chemistry: a patent review (2010-2015). *Expert Opin. Ther. Pat.* **2017**, 27, 63−79.

(11) Hu, G. Q.; Wu, X. K.; Wang, G. Q.; Duan, N. N.; Wen, X. Y.; Cao, T. Y.; Jun, Y.; Wei, W.; Xie, S. Q.; Huang, W. L. Synthesis and antitumor and antibacterial evaluation of fluoro-quinolone derivatives (III): mono- and bis-Schiff-bases. *Chin. Chem. Lett.* **2012**, 23, 515−517.

(12) Ren, S.; Wang, R.; Komatsu, K.; Bonaz-Krause, P.; Zyrianov, Y.; McKenna, C. E.; Csipke, C.; Tokes, Z. A.; Lien, E. J. Synthesis, biological evaluation, and quantitative structure-activity relationship analysis of new Schiff bases of hydroxysemicarbazide as potential antitumor agents. *J. Med. Chem.* **2002**, 45, 410−419.

(13) Hearn, M. J.; Cynamon, M. H. Design and synthesis of antituberculars: preparation and evaluation against mycobacterium tuberculosis of an isoniazid Schiff base. *J. Antimicrob. Chemother.* **2004**, 53, 185−191.

(14) Silva, C. D.; Silva, D. D.; Modolo, L. V.; Alves, R. B.; Resende, M. D.; Martins, C. V.; Fatima, A. D. Schiff bases: a short review of their antimicrobial activities. *J. Adv. Res.* **2011**, 2, 1−8.

(15) Murtaza, S.; Akhtar, M. S.; Kanwal, F.; Abbas, A.; Ashiq, S.; Shamim, S. Synthesis and biological evaluation of schiff bases of 4-aminophenazone as an anti-inflammatory, analgesic and antipyretic agent. *J. Saudi Chem. Soc.* **2017**, 21, S359−S372.

(16) Sztanke, K.; Maziarka, A.; Osinka, A.; Sztanke, M. An insight into synthetic Schiff bases revealing antiproliferative activities *in vitro*. *Bioorg. Med. Chem.* **2013**, 21, 3648−3666.

(17) Rauf, A.; Shah, A.; Munawar, K. S.; Khan, A. A.; Abbasi, R.; Yameen, M. A.; Khan, A. M.; Khan, A. R.; Qureshi, I. Z.; Kraatz, H. B. Synthesis, spectroscopic characterization, DFT optimization and biological activities of Schiff bases and their metal(II) complexes. *J. Mol. Struct.* **2017**, 1145, 132−140.

(18) Zhao, F.; Liu, Z. Q. The protective effect of hydroxyl-substituted Schiff bases on the radical-induced oxidation of DNA. *J. Phys. Org. Chem.* **2009**, 22, 791−798.

(19) Heck, M.; Schädel, S. A.; Maretzki, D.; Bartl, F. J.; Ritter, E.; Palczewski, K.; Hofmann, K. P. Signaling states of rhodopsin formation of the storage form, metarhodopsin III, from active metarhodopsin II. *J. Biol. Chem.* **2003**, 278, 3162−3169.

(20) Soderberg, T. *Organic Chemistry with a Biological Emphasis Volume I*. Chemistry Publications **2016**.

(21) Naderi, E.; Ehteshamzadeh, M.; Jafari, A. H.; Hosseini, M. G. Effect of carbon steel microstructure and molecular structure of two new Schiff base compounds on inhibition performance in 1M HCl solution by DC, SEM and XRD studies. *Mater. Chem. Phys.* **2010**, 120, 134−141.

(22) Khuhawar, M. Y.; Mughal, M. A.; Channar, A. H. Synthesis and characterization of some new Schiff base polymers. *Eur. Polym. J.* **2004**, 40, 805−809.

(23) Rakesh, K. P.; Manukumar, H. M.; Gowda, D. C. Schiff's bases of quinazolinone derivatives: synthesis and SAR studies of a novel series of potential anti-inflammatory and antioxidants. *Bioorg. Med. Chem. Lett.* **2015**, 25, 1072−1077.

(24) Kumar, D.; Rawat, D. S. Synthesis and antioxidant activity of thymol and carvacrol based Schiff bases. *Bioorg. Med. Chem.* **2013**, 23, 641−645.

(25) Khan, K. M.; Khan, M.; Ali, M.; Taha, M.; Rasheed, S.; Perveen, S.; Choudhary, M. I. Synthesis of bis-Schiff bases of isatins and their antiglycation activity. *Bioorg. Med. Chem.* **2009**, 17, 7795–7801.

(26) Vančo, J.; Marek, J.; Trávníček, Z.; Račanská, E.; Muselík, J.; Švajlenová, O. G. Synthesis, structural characterization, antiradical and antidiabetic activities of copper(II) and zinc(II) Schiff base complexes derived from salicylaldehyde and *β*-alanine. *J. Inorg. Biochem.* **2008**, 102, 595–605.

(27) Kia, R.; Kargar, H. Crystal structure, spectroscopic characterization, and computational study of two new 4-aminobenzoic acid derived Schiff base ligands. *Sci. Iran. Trans. C, Chem. Chem. Eng.* **2015**, 22, 2298–2308.

(28) Rauf, A.; Shah, A.; Khan, A. A.; Shah, A. H.; Abbasi, R.; Qureshi, I. Z.; Ali, S. Synthesis, pH dependent photometric and electrochemical investigation, redox mechanism and biological applications of novel Schiff base and its metallic derivatives. *Spectrochim. Acta Part A: Mol. Biomol. Spectr.* **2017**, 176, 155–167.

(29) Meotti, F. C.; Borges, V. C.; Zeni, G.; Rocha, J. B.; Nogueira, C. W. Potential renal and hepatic toxicity of diphenyl diselenide, diphenyl ditelluride and Ebselen for rats and mice. *Toxicol. Lett.* **2003**, 143, 9–16.

(30) Mehmood, S.; Rehman, M. A.; Ismail, H.; Mirza, B.; Bhatti, A. S. Significance of postgrowth processing of ZnO nanostructures on antibacterial activity against gram-positive and gram-negative bacteria. *Int. J. Nanomed.* **2015**, 10, 4521–4533.

(31) *Molecular Operating Environment* (MOE), 2016.08; Chemical Computing Group Inc., 1010 Sherbrooke St. West, Suite #910, Montreal, QC, Canada, H3A 2R7 2016.

(32) Vicens, Q.; Westhof, E. Crystal structure of paromomycin docked into the eubacterial ribosomal decoding A site. *Structure* **2001**, 9, 647–658.

(33) Rehman, A. U.; Khan, M. T.; Liu, H.; Wadood, A.; Malik, S. I.; Chen, H. F. Exploring the pyrazinamide drug resistance mechanism of clinical mutants T370p and W403g in ribosomal protein S1 of mycobacterium tuberculosis. *J. Chem. Inf. Model.* **2019**, 59, 1584–1597.

(34) Rehman, A. U.; Rafiq, H.; Rahman, M. U.; Li, J.; Liu, H.; Luo, S.; Arshad, T.; Wadood, A.; Chen, H. F. Gain-of-function SHP2 E76Q mutant recusing autoinhibition mechanism associated with juvenile myelomonocytic leukemia. *J. Chem. Inf. Model.* **2019**, 59, 3229–3239.